# Electrostatically trapping indirect excitons in coupled $In_xGa_{1-x}As$ quantum wells

G. J. Schinner, E. Schubert, M. P. Stallhofer, and J. P. Kotthaus

*Center for NanoScience and Fakultät für Physik, Ludwig-Maximilians-Universität, Geschwister-Scholl-Platz 1, D-80539 München, Germany*

D. Schuh

*Institut für Experimentelle Physik, Universität Regensburg, D-93040 Regensburg, Germany*

A. K. Rai, D. Reuter, and A. D. Wieck

*Angewandte Festkörperphysik, Ruhr-Universität Bochum, Universitätsstraße 150, D-44780 Bochum, Germany*

A. O. Govorov

*Department of Physics and Astronomy, Ohio University, Athens, Ohio 45701, USA*
*Center for NanoScience and Fakultät für Physik, Ludwig-Maximilians-Universität, Geschwister-Scholl-Platz 1, D-80539 München, Germany*

We report on photoluminescence experiments on spatially indirect excitons in an InGaAs coupled double quantum well device in which semitransparent gates are employed to tune the in-plane potential landscape. We introduce a trapping configuration in which exciton generation is spatially separated from the excitonic trapping potential. Suitably biased gates control the flow of indirect dipolar excitons from the generation area to the electrostatically defined trap. Thus the trap is filled only with indirect excitons precooled to the lattice temperature. Using a confocal microscope at liquid helium temperatures we map the in-plane distribution of excitons at various gate voltages and illumination conditions. Our small and strongly confining traps with precooled excitons demonstrate interesting many-body effects which can be interpreted in terms of the electrostatic screening, the Coulomb binding, and excitonic flows. Gate voltage dependencies of PL energy in our samples are not monotonic and can be explained by considering the nonlinear exciton flows between the elements of our structure. At strong illumination hysteretic switching of the trapped exciton population reflects a nonlinear character of the self-consistent trapping potential. An unusual nonlinear increase of the emission of the trap is likely coming from the many-body interactions in a dense exciton gas in the presence of a disorder potential at high light intensity. The designs of electrostatic traps proposed and realized here allow for stronger confinements and lower temperatures and will be used to search for coherent phenomena in dense exciton gases.

## I. INTRODUCTION

Spatially indirect excitons (IX) are bound electron hole pairs consisting of an electron and a hole spatially separated in two adjacent quantum wells. The constituents of the exciton are fermions, but the bound state builds a boson. Bose-Einstein condensation (BEC) of excitons, though predicted by Keldysh and Kozlov decades ago,[1] deserves further experimental exploration beyond recent experiments[2,3] reporting spatial coherence of indirect excitons in coupled quantum wells (CDQW). Such dipolar excitons form a complicated bosonic system of dipolar and interacting quasiparticles with an inner structure and a tunable lifetime exposed to a disorder potential.

BEC has been observed in superconductors, superfluids, and ultracold diluted atomic gases in the last century. More recently, condensation of nonequilibrium quasiparticles in solids, namely magnons[4] and exciton polaritons,[5,6] have been reported as other examples of BEC. To achieve a BEC of excitons confined in the 2D plane of the heterostructure, an efficient trapping of high exciton densities thermalized to cryogenic temperatures is required.[7,8] With different approaches such exciton traps have been realized within the last years. They include strain-induced traps,[9–11] natural traps due to disorder in the QW plane,[12] magnetic traps,[13] traps generated by surface acoustic waves,[14] and laser-induced traps.[15] The most promising and widely tunable exciton traps rely on

the electrostatically induced quantum confined Stark effect (QCSE).[16–24] They were realized in various geometries and with different trapping efficiencies. Excitonic traps can also combine the electrostatic confinement and the strain-induced localization. Such traps were realized using silicon dioxide.[25] They provide a strong confinement along the perimeter around a $SiO_2$ patch and allow the exciton gas a one-dimensional expansion over very long distances.[26]

Here, we utilize a trap configuration in which the exciton generation is separated spatially far from the trapping potential and the confinement potential of the trap can be tuned widely with independently biased gates. Thus the trap is filled only with indirect excitons, precooled to the lattice temperature and acquiring only a small well-controlled excess energy when entering the trap. This is in contrast to the majority of traps previously realized. Using spatially resolved photoluminescence (PL) we demonstrate the operating principle. We are able to fully control the in-plane exciton gas dynamics by suitably chosen voltages applied to the gates. We report how each gate influences the exciton behavior when the applied bias is changed. Additionally, it is possible to use a nonlinear trapping configuration to switch the exciton population and we present the characteristics of switching the IX flow. Furthermore, we observe and interpret an unexpected nonlinear increase of the PL intensity with the trapped IX density.

## II. SPATIALLY INDIRECT EXCITONS IN VOLTAGE-TUNED COUPLED DOUBLE QUANTUM WELLS

In our experiments on spatially indirect excitons we employ double quantum wells embedded within a field-effect tunable diode structure. A schematic of the band diagram is displayed in Fig. 1(a). Two narrow $In_{0.11}Ga_{0.89}As$ quantum wells, separated by a center to center distance $d$ comparable to the excitonic Bohr radius $a_B \approx 20$ nm, are embedded between an $n$-doped GaAs back contact and a semitransparent gate electrode. Without bias, midgap states at the surface of the GaAs-based heterostructure are the cause of a built-in electric field perpendicular to the CDQW plane, which raises the conduction band energy at the heterojunction-gate interface by about 0.7 eV, half the band gap of GaAs. With laser illumination at an energy above the band gap of GaAs, we create electron-hole pairs which relax via optical and acoustic phonon emission on a subnanosecond timescale to form both direct excitons (DX) within one of the quantum wells and spatially indirect excitons in which the electron and hole are separated by a distance of about the center to center distance of the DQW.[27–29] Whereas the direct excitons recombine on a nanoseconds time scale,[30] the indirect excitons exhibit life times up to microseconds[31] which are determined by the spatial overlap of the electron and hole wave function. The binding energy of the indirect exciton is dominated by the DQW distance $d$ and at $d \sim a_B$ is only weakly dependent on the wave function overlap.[32] The IX form dipoles with dipole moment $p = ed$ oriented perpendicular to the QW plane. As long as their in-plane separation $l = \frac{1}{\sqrt{n_{IX}}}$, where $n_{IX}$ denotes the excitonic density, is larger than $a_B$, their dipolar repulsion prevents a Mott transition to a metallic electron-hole double layer plasma.[33] Since the recombination lifetime of the IX is significantly longer than the energy relaxation time to the excitonic ground state, the IX are likely to cool down to lattice temperature before recombining. This makes them particularly suitable for studies aimed at BEC.

The motion of IX within the QW plane is driven by gradients of both the effective excitonic potential $V_{IX}$ and density $n_{IX}$ and, furthermore, by dipolar repulsion forces between excitons. The potential $V_{IX}$ is formed by the biased gates and also includes a disorder component. To aim for the excitonic BEC it is necessary to create traps within the QW plane to spatially confine excitons. We employ the easy voltage tunability of the quantum-confined Stark effect to create a landscape for the in-plane excitonic potential that guides IX to a tunable trap, conceptually similar to what is employed in BEC of atomic systems. The QCSE causes a redshift of the excitonic energy of $\Delta E_{IX} = pF$, where $F$ is the effective electric field perpendicular to the QW plane. At sufficiently low $n_{IX}$ and for a large diameter gate with $D \gg d$, this is determined solely by the capacitance of the field-effect device and is $F = \frac{1}{l_0}(V_g - V_{FB})$, where $V_{FB}$ corresponds to the flat-band voltage, at which the external voltage compensates the built-in electric field, and $l_0$ denotes the lever arm, i.e., the distance between the gate and the embedded $n$-doped back contact. In the case of high IX densities, especially for trapped IX, a large ensemble of IX partially screens the externally applied electric field via their dipole interaction. The
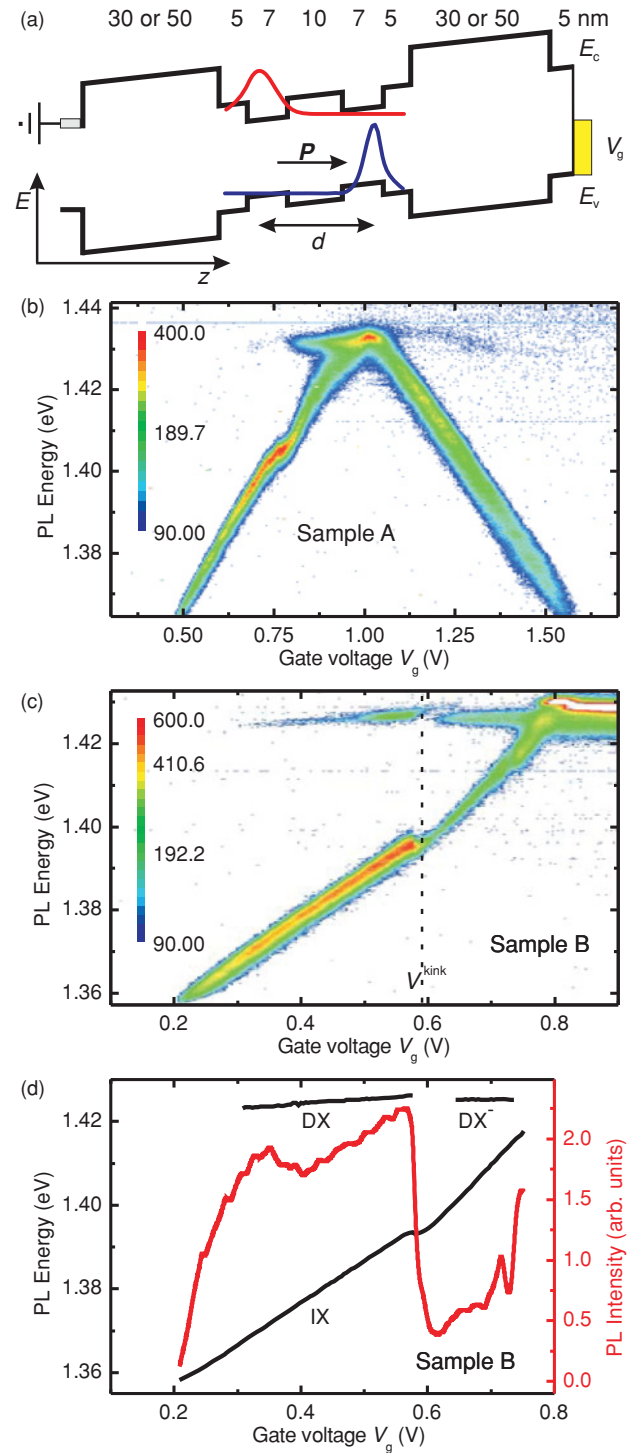


FIG. 1. (Color online) (a) Schematic of the CDQW band gap within a field-effect device with numbers indicating the layer thickness of the InGaAs QWs, the GaAs spacers, and the AlGaAs barriers, respectively. $E_c$ and $E_v$ denote the conduction and valence band edge, respectively. (b) PL measurement of the QCSE of sample A and sample B (c) with a homogeneous unstructured gate. In (b) and (c), the PL intensity is displayed in a logarithmic color scale and plotted as a function of the PL energy and the applied bias $V_g$. In (d), the PL peak energies of direct (DX) and spatially indirect (IX) excitons (black, left axis) and the integrated intensity of the IX PL (red, right axis) of the measurement (c) are shown as a function of the gate voltage $V_g$.

consequence is a blueshift $\Delta E$ of the IX energy, because the effective electric field is reduced. A different way to understand this blueshift is the IX-IX interaction. The IX gas influences the $V_{IX}$ seen by the individual IX at a constant gate voltage $V_g$. For not too small IX densities $n_{IX}$, it is possible to well approximate

$$n_{IX} = \frac{\epsilon_0 \epsilon \, \Delta E}{e^2 d} \qquad (1)$$

with the measured blueshift $\Delta E$, and $\epsilon_0 \epsilon$ are the vacuum and relative dielectric constants, respectively.[34] This linear relation is likely to underestimate the total IX density by about $2 \times 10^{10} \, \frac{1}{cm^2}$ as discussed in more detail in Ref. [35].

In the following we discuss the QCSE for a large area homogeneous gate observed in our $In_x Ga_{1-x} As$ CDQW. The heterostructures employed are a CDQW field-effect device with an $n$-doped back contact grown by molecular beam epitaxy on a GaAs substrate polished on both sides. The two InGaAs quantum wells with 7 nm width are separated by a 10 nm GaAs tunnel barrier. The active layer is surrounded by two symmetric spacer layers [see Fig. 1(b)]. In sample A we used 30 nm AlGaAs and in sample B 50 nm thick GaAs-AlAs short period superlattices (SPS) as spacers.

Figure 1(b) shows the QCSE of sample A under a homogeneous gate. Plotted is the PL intensity in a logarithmic color scale as a function of the PL energy and applied gate voltage $V_g$. The PL is measured at a bath temperature of 4 K in the focus of the exciton generation with a 633 nm (1.959 eV) pump laser operating at power $P_{laser} = 80$ nW. Figure 1(c) shows a comparable measurement on sample B. For a more quantitative analysis Fig. 1(d) displays the data of Fig. 1(c), giving both the PL peak energies of IX and DX (black, left-hand axis) and integrated intensity (red, right-hand axis) of the IX PL as a function of gate voltage $V_g$. At flat band, when the electrical field in the field-effect device vanishes, the electronic ground state of the InGaAs DQW is below the chemical potential of the back contact. At the gate voltage $V_{kink}$ at which the electron ground state of the IX in the lower QW coincides with the Fermi energy of the back contact, the linear QCSE shows a kink. At voltage $V_g < V_{kink}$, the IX PL energy is blueshifted and the IX PL intensity shows a steep increase [see red trace in Fig. 1(d)]. In sample A with barriers on both sides of the CDQW made of $Al_x Ga_{1-x} As$ ($x = 0.42$) the QCSE is observable for voltage $V_g$ both below and above $V_{FB}$ [Fig. 1(b)]. In sample B where the alloy is replaced by a SPS barrier as described above, charge storage in the QW under illumination prevents the observation of the QCSE $V_g > V_{FB}$, because the externally applied electric field is completely screened. Both samples show also a weak but discernible PL of direct excitons. In sample B and at $V_g > V_{kink}$, at which the QW electronic ground state is below Fermi energy of the back contact, we see PL of trion excitons. The trion is a negatively charged $DX^-$ caused by the free electrons stored in the QW when $V_g > V_{kink}$. As expected the $DX^-$ is observed at lower energy than the DX and found to be independent of $V_g$ at $V_g > V_{kink}$. In contrast, for $V_g < V_{kink}$, the direct exciton PL energy shows a red shift with increased electric field of 11 $\frac{meV}{V}$. On sample A, with AlGaAs alloy barriers, we observe a weak direct exciton PL, but we are unable to detect PL from $DX^-$ at any laser power and excitation wavelength (830 nm, 808 nm, and 633 nm). We interpret the different behavior

of the two heterostructures by charge storage in sample B. Whenever the electronic ground state in the CDQW drops below the Fermi energy of the back contact, electrons can be collected in the CDQW. We then observe the trion formation, and screening of the gate-induced field prevents a finite QCSE for $V_g \gtrsim V_{FB}$.

The trap discussed in the next section is strongly influenced by the kink in the QCSE at $V_g = V_{kink}$. For the trap functionality, IX diffusion is important and depends critically on the gate voltage $V_g$. Therefore we investigate the IX diffusion on a large homogenous gate. We generate IX in the focus of a 830 nm (1.494 eV) pump laser (9 $\mu$W). With spatially resolved PL measurements (not shown here) we find that for a gate voltage $V_g = 0.60$ V $> V_{kink}$, the IX intensity is halved after 9 $\mu$m, whereas for $V_g = 0.50$ V $< V_{kink}$ the IX intensity is halved after 24 $\mu$m. This indicates a rather sudden increase of the lifetime of IX at $V_g \lesssim V_{kink}$. Correspondingly, we see in Fig. 1(d) a strong increase in the IX PL intensity and IX density.

## III. SPATIALLY RESOLVED PHOTOLUMINESCENCE FROM A CHUTE TRAP

By a lateral modulation of the electric field applied perpendicular to the quantum well plane it is possible to create an arbitrary potential landscape for (indirect) excitons. Using adequate gate geometries and applied voltages it is possible to gain full control over the exciton in-plane dynamics. To achieve a perfect exciton trapping the location of the DQW inside the heterostructure is important.[19] We have positioned the DQW in the middle of the field-effect device, because of the exponential decay of the Fourier components of the in-plane potential with increasing distance from surface gates defining the trap geometry. We use sample B with 50 nm GaAs-AlAs SPS barriers to build traps. The back contact is contacted by an ohmic contact and the surface gates are laterally patterned using $e$-beam lithography. The GaAs substrate is transparent for the CDQW PL light of the InGaAs QWs because the corresponding photon energy is below the GaAs band gap. For our spatially resolved studies we use a confocal microscope with two objectives operating at liquid helium temperatures.[36] The objective on top of the sample is used to excite IX with 1.494 eV (830 nm) laser energy. The second objective below the sample is used to collect the PL light in transmission and analyze it in a spectrometer. Both objectives are diffraction limited and thus have a focus spot size with a diameter comparable to the wavelength and can be individually positioned with piezoactuators. Additionally it is possible to apply magnetic fields up to 14 T perpendicular to the QW plane.

With the aim of studying the PL of fully confined IX in thermal equilibrium with the lattice and without the perturbation of emission by DX and impurity transitions generated in the focus area of the incident laser radiation, we developed a chutelike trapping configuration displayed in Fig. 2(b). It has three gates with a circular gate with bias $V_T$ defining a trap for IX, a slide gate with bias $V_S$ on which we optically generate electron-hole pairs as indicated by the red spot in Fig. 2(b), and an outside surrounding guardlike gate with bias $V_G$ which defines the excitonic confining potential

in the area surrounding the trap and slide. The semitransparent gates are 6 nm thick evaporated Ti films and are separated by narrow ungated slits, visible as long gray lines in Fig. 2(b) which are only about 100 nm wide. They are narrow to prevent ill-defined potentials which are caused by charges on open GaAs surfaces and can form barriers preventing exciton transport from, e.g., the slide gate to the trap gate.

Figure 2(c) shows a schematic sketch of the exciton potential landscape $V_{IX}$ along the $x$ direction of the chute trap when $V_T < V_S < V_G$. With illumination on the slide gate, IX generated in the laser focus are expanding on the slide driven by diffusion and dipolar repulsion and are attracted by the energetically deeper exciton potential under the suitably biased trap gate. With suitable bias, the device acts like a chute which transports IX from the point of generation into the trap with the latter essentially not exposed to electron-hole generating radiation by virtue of the two separate confocal optics employed in our low temperature microscope.

Figure 2(d) illustrates the corresponding energy landscape for the electron and hole states forming the indirect exciton in the InGaAs DQW. Note that the trapping potential in this bias configuration $V_T < V_S < V_G$ only is effective for IX. The potential step at the trap edge can only be overcome by bound indirect excitons. Direct excitons are likely to recombine before reaching the trap and unbound electrons are repelled from the trap as illustrated in Fig. 2(d).

Spatially and energetically resolved PL images obtained with the collection objective moving along $y$ and $x$ directions are displayed in Figs. 2(a) and Fig. 2(e), respectively. Figure 2(a) plots the PL energy against $y$ for a section through the middle of the trap at $x = 0$ with the PL intensity logarithmically color coded. The same data are illustrated in a pseudo-3D Fig. 2(f) with a linear PL intensity scale. The excitonic cloud is perfectly trapped and the spatial width of the PL intensity at half maximum is 5.5 $\mu$m whereas the diameter of the trap gate is 6.0 $\mu$m. Solving the Laplace equation yields a boxlike excitonic potential with 5.5 $\mu$m diameter, identical to the measured PL spatial width. In this trap configuration it is possible to realize ideal trapping and we are able to control the in-plane exciton dynamics.

Figure 2(e) displays the PL energy along $x$ in a cut through the middle of the trap ($y = 0$) as indicated by the red line in Fig. 2(b) with the PL intensity again color coded logarithmically. The exciton generation by the pump laser occurs about 9 $\mu$m away from the trap center. In close vicinity to the pump laser focus, indirect excitons form within very short relaxation and cool-down times.[29] Afterward, they diffuse into the energetically favored trapping area. Indirect excitons can easily transcend the gap between the slide and trap gate. As reflected in Fig. 2, the trap is homogeneously filled with indirect excitons, with no detectable leakage at the trap gate lead. The energetically highest PL signals in
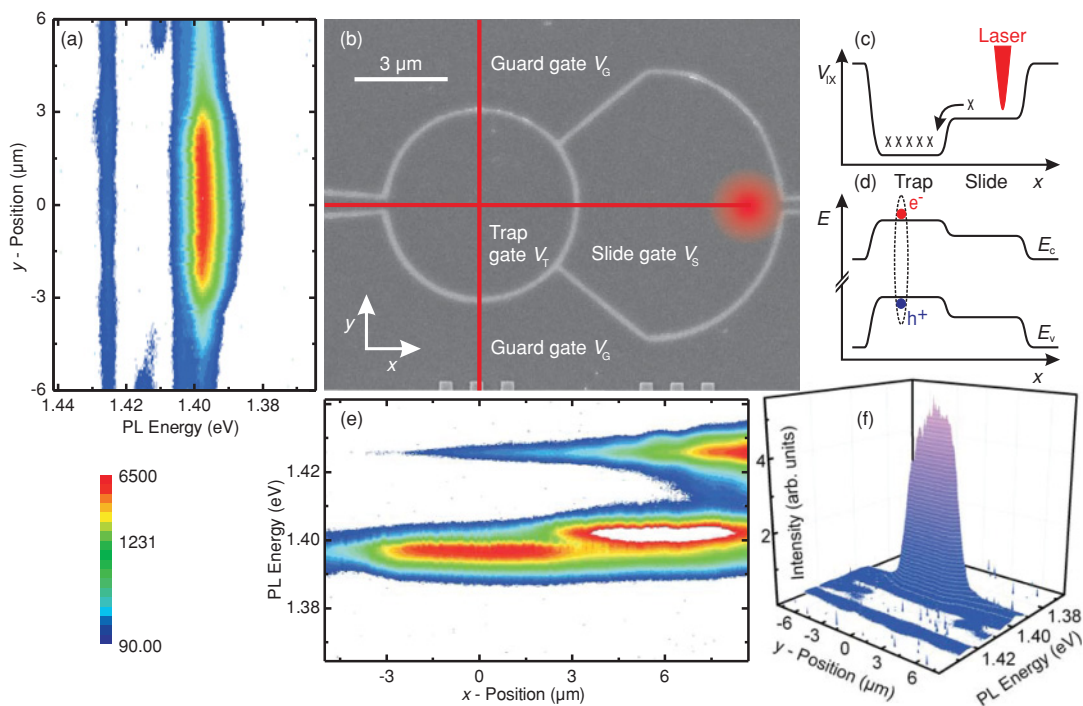


FIG. 2. (Color online) The figure shows spatially and energy resolved measurements of the exciton expansion in the chute trap. In (a) and (e) cuts are shown of the PL intensity in a logarithmic color scale, given by the scale bar on the lower left, as a function of the position and PL energy. The data are measured along the red lines in the scanning electron micrograph shown in (b) of the trapping configuration which is composed of a slide, trap, and guard gate. The pump laser position is fixed on the slide gate as indicated by the bright spot in (b). In (c) a schematic drawing of the exciton potential landscape of the chute trap is displayed. In (d) the corresponding energies of the conduction $E_c$ and valence band edge $E_v$ of the InGaAs CDQW are illustrated. The pseudo-3D picture (f) illustrates the same data as shown in (a) with a linear intensity axis. Here, the voltages applied are $V_G = 0.7$ V on the guard gate, $V_T = 0.35$ V on the trap gate, and $V_S = 0.45$ V on the slide gate. The temperature was 4 K and the laser power 8.0 $\mu$W at 1.494 eV energy.

Figs. 2(a), 2(e), and 2(f) stem from direct excitons. Because of their short lifetime they decay within 1 $\mu$m distance from the excitation focus to half their intensity and are weakly detected by the collection objective. In the excitation focus, the indirect exciton recombination is strongly suppressed. This we interpret to result, at least partially, from the high kinetic energy and momentum of IX that prevents radiative recombination because of conservation laws.[29] In contrast to observations in Ref. 37 we find no indications for the presence of an electron-hole plasma. We also observe in Figs. 2(a), 2(e), and 2(f) no PL from a DX$^-$.

## IV. VOLTAGE TUNABILITY OF THE EXCITONIC POTENTIAL OF THE CHUTE TRAP

In the following we discuss how the trap can be tuned by the three gate voltages. In these experiments the pump laser (1.494 eV) is focused on the slide gate at a fixed position as indicated in Fig. 2(b). The PL is collected from the center of the trap gate.

### A. Electrical currents

Before discussing the action of the gate voltages on the PL spectra we briefly want to discuss the characteristic dependencies of leakage currents in the device. We have measured the electrical current flow onto the gates and to the back contact. To generate electron-hole pairs we use a laser (1.494 eV) with a relatively high laser power of 28 $\mu$W focused on the slide gate. All three gates are changed in parallel with a constant voltage offset to the trap gate of $V_S - V_T = 0.1$ V and $V_G - V_T = 0.2$ V. The current $I_T$ onto the trap gate (A, left black axis in Fig. 3) is always smaller than 100 pA. Trace (B) in Fig. 3 corresponds to a current $I_G$ flowing onto the guard gate. For a smaller guard gate voltage $V_G < 0.25$ V $I_G$ rises but remains very weak. On the slide gate we observe a strong current $I_S$ for a slide gate voltage below $V_S < 0.2$ V (D and right red axis in Fig. 3). $I_S$ also becomes the main contribution to the current out of the back contact
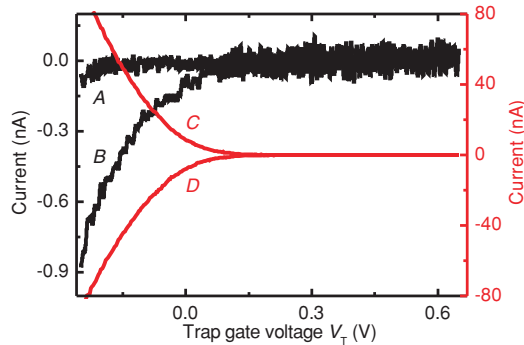


FIG. 3. (Color online) Electrical current flow on the gates and to the back contact. The pump laser (1.494 eV) is fixed on the slide gate [as in Fig. 2(b)] with very high laser power 28 $\mu$W. All three gates are shifted parallel with a constant voltage offset to the trap gate of $V_S - V_T = 0.1$ V and $V_G - V_T = 0.2$ V. Trace (A) is the current on the trap gate (black left-hand axis). (B) labels the current on the guard gate. On the right red current axis, the current of the back contact (C) and of the slide gate (D) is plotted.

$I_B$ (C) in Fig. 3 with $I_B = I_S + I_T + I_G$. In the voltage range where we operate the trap and with the laser powers used (normally much less than 28 $\mu$W), there are no discernible currents between the gates. We thus can rely on the externally applied voltages fully reflecting the potentials applied at the gates.

### B. Dependence on each gate voltage

Under variation of the trap gate voltage $V_T$ at fixed $V_S = 0.5$ V and $V_G = 0.8$ V the IX change their energy and integrated intensity as displayed in Fig. 4(a). The excitons are generated on the slide gate and the PL is collected from the trap center.
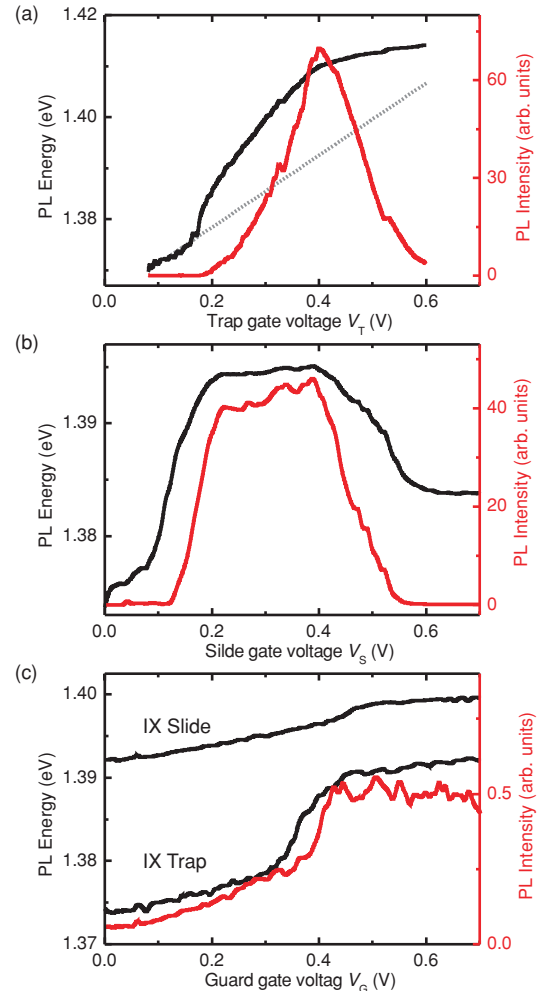


FIG. 4. (Color online) The action of each gate voltage on the PL of IX in the trap is displayed. The excitons are generated at energy of 1.494 eV ($\lambda = 830$ nm) on the slide gate as in Fig. 2(b) and the PL is detected from the trap center. Plotted is the PL energy (black, left-hand side) and the integrated PL intensity of IX (red, right-hand side) as a function of the respective gate voltage with the other gates voltages constant. In (a) the $V_T$ is varied at constant $V_G = 0.8$ V and $V_S = 0.5$ V (laser power 30 $\mu$W). In (b) the slide gate voltage $V_S$ is varied at constant $V_G = 0.8$ V and $V_T = 0.35$ V (laser power 7 $\mu$W). In (c) is shown the dependence on the guard gate voltage $V_G$ at constant $V_S = 0.45$ V and $V_T = 0.35$ V (laser power 7 $\mu$W). In (c), the IX PL energy from the slide gate area is plotted in addition.

With decreasing $V_T$ it is possible to increase the effective trap depth up to 30 meV. Raising $V_T$ from 0.1 V to 0.6 V the PL energy in Fig. 4(a) increases faster than the linear QCSE as indicated by the dotted line which is an extension of a linear fit for 0.08 V$< V_T <$ 0.18 V with a slope of 71 $\frac{\text{meV}}{\text{V}}$. This strong blueshift reflects the increasing exciton density in the trap. With increasing trap gate bias $V_T$, the PL intensity [red, right-hand side scale in Fig. 4(a)] rises from almost vanishing to a maximum value which is reached at $V_T \approx 0.4$ V where also the PL blueshift is maximal. Further increasing trap gate voltage yields an excitonic potential that is higher than the one under the slide gate and the PL intensity decreases strongly as IX no longer fill the trap. We name this configuration an antitrap.

Figure 4(b) shows the PL behavior of IX from the trap center with changing $V_S$ at constant $V_T = 0.35$ V, $V_G = 0.8$ V. The PL energy for $V_S > 0.6$ V is constant. By varying the voltage on the slide gate the generation of IX on the slide gate is strongly enhanced for voltages $V_S < 0.6$ V $< V_{\text{kink}}$ [see Fig. 1(c)], and the trap is effectively filled with excitons. For 0.15 V $\lesssim V_S \lesssim$ 0.6 V, the PL energy in the trap is blueshifted and the PL intensity enhanced. Further decreasing $V_S$ results in an antitrap and correspondingly causes the exciton density of IX in the trap to rapidly vanish.

Figure 4(c) displays the dependence of the IX PL from both the trap and slide area, on guard gate voltage $V_G$ at fixed $V_T = 0.35$ V and $V_S = 0.45$ V. Here, the PL energies from the slide (upper trace) and trap gate are plotted as functions of the guard gate voltage. In addition, it shows the PL intensity from the trap center in red as given by the right-hand side of Fig. 4(c). As the guard gate voltage $V_G$ is reduced from 0.7 V to 0.5 V, the exciton energy and the corresponding density below the slide and trap gate are essentially constant. Once $V_G$ drops below $V_S$, IX preferentially flow from the slide to the guard gate. This results in a reduction of the exciton energy and density on the slide gate. Consequently, the reduced confinement at around $V_G \simeq 0.2$ V causes a redshift of the trap PL of about 15 meV, corresponding to a drop in density of roughly $7 \times 10^{10}$ $\frac{1}{\text{cm}^2}$. In comparison, one observes a much weaker decrease of the PL energy on the slide gate with decreasing $V_G$, reflecting the nearly constant density in the area where excitons are generated. The influence of the guard gate demonstrates that the trap design is well suited to collect and confine exciton densities up to high densities of order $10^{11}$ $\frac{1}{\text{cm}^2}$.

Another experimental finding that characterizes the function of the trap design is summarized in Fig. 5. Here, the trap gate voltage $V_T$ is changed simultaneously with $V_G$ and $V_S$ with the offset $\Delta V = V_S - V_T$ as parameter whereas $V_G - V_S = 0.2$ V is kept constant. In Fig. 5(a) the variation of the PL energy with $V_T$ is logarithmically color coded for the case $\Delta V = 0.25$ V. The energetically lowest PL branch results from the trap. For trap voltages larger than $V_T > 0.33$ V the PL intensity is weak. With decreasing trap gate voltage $V_T$, the PL energy shows a strong blueshift while the PL intensity grows abruptly. This reflects the sudden enhancement of the exciton density at $V_T = 0.33$ V. At this value of $V_T$, corresponding to $V_S = 0.58$ V, efficient generation of indirect excitons on the slide gate which drift into the trap begins. This can be deduced from the next higher PL branch in Fig. 5(a) which
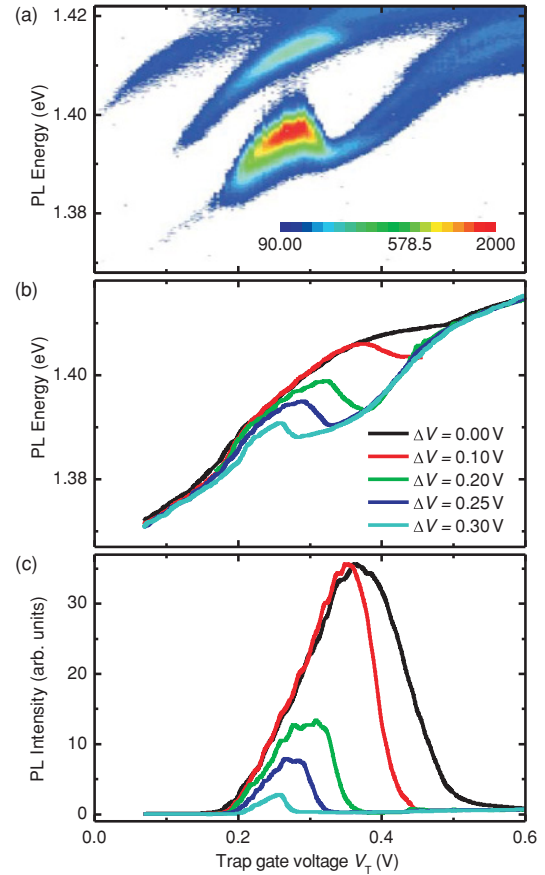


FIG. 5. (Color online) (a) Trap PL dependence with all gate voltages varied simultaneously at constant offset $\Delta V = V_S - V_T = 0.25$ V and $V_G - V_T = 0.45$ V. The energy resolved PL intensity is logarithmically plotted as function of the trap gate voltage. The energetically lowest PL branch is the PL from the trap. Above weak PL signals from the slide and guard gate area are discernible. In (b) is plotted the PL peak energy of the trap for different voltage offsets $\Delta V = V_S - V_T$. The voltage difference between guard and slide gate is always $V_G - V_S = 0.2$ V. In (c) is shown the corresponding PL intensity collected in the trap. The incident laser power is 20 $\mu$W.

results from the PL on the slide gate that enters the objective. Once the QCSE enables, at $V_S < 0.58$ V, spatial separation of photogenerated electron-hole pairs in the CDQW on the slide, the PL energy on the slide decreases and simultaneously the slide PL intensity increases. This is in perfect agreement with the experiments on sample B with a homogenous gate, displayed in Figs. 1(c) and 1(d). As the offset voltage $\Delta V$ is varied the corresponding onset of the filling of the trap is seen in the PL energy versus $V_T$ traces in Fig. 5(b). The accompanying increase in the exciton density is reflected by the increase in PL intensity with $\Delta V$ shown in Fig. 5(c).

With increasing offset $\Delta V$, the region where the trap gets effectively filled with excitons shifts to lower trap gate voltages as a consequence of the voltage dependence generation of IX on the slide gate. The uppermost curve reflects the maximal filling with the laser power used here (20 $\mu$W). In contrast the lowest trace in Fig. 5(c) provides the case of a low exciton density in the trap. Once a blueshift is noticeable in Fig. 5(b) we observe an increased PL intensity in Fig. 5(c).
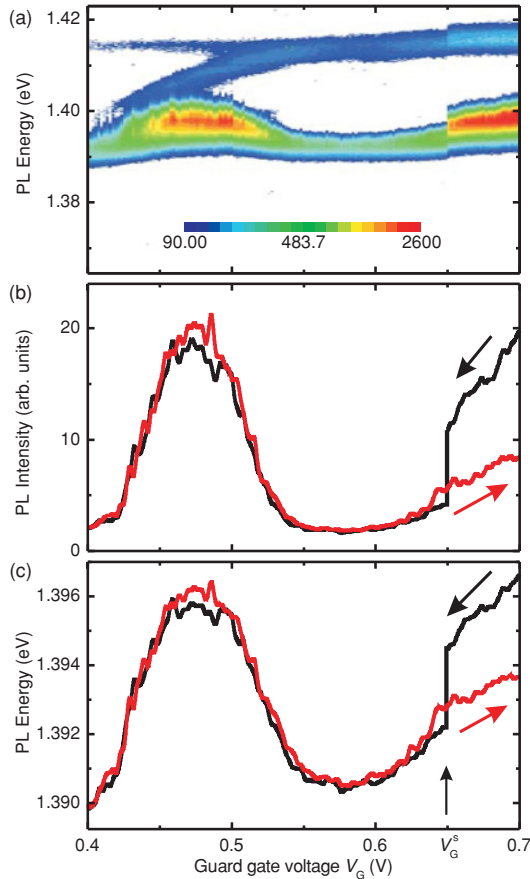
FIG. 6. (Color online) The exciton potential below the guard gate is varied. For the case of high excitation power (20 $\mu$W) and with the slide gate voltage slightly smaller than the kink voltage of the QCSE we observe a steplike change of the trapped exciton density. In (a) the PL intensity is plotted logarithmically as a function of the PL energy and the decreasing guard gate voltage. In (b) and (c) are shown the corresponding PL intensity energy of the trapped indirect excitons for both sweep directions of $V_G$. The trap gate voltage is $V_T = 0.35$ V and the slide gate voltage $V_S = 0.55$ V.

## V. HYSTERETIC SWITCHING OF THE TRAPPED EXCITON DENSITY

At a sufficiently high generation rate of indirect excitons, we surprisingly observe a hysteretic behavior of the exciton population in the trap. As in the experiment discussed above, the trap gate is biased at a voltage below the one of the slide gate and indirect excitons are generated in the focus spot on the slide gate while PL is detected from the center of the trap gate. At $V_T = 0.35$ V, $V_S = 0.55$ V, and an illumination power of 20 $\mu$W at a laser energy of 1.494 eV, the detected PL exhibits a sudden change with decreasing $V_G$ as illustrated in Fig. 6(a), where the PL energy is displayed with its intensity logarithmically color coded. The slide gate voltage is chosen to be slightly below the kink voltage $V_{kink}$ in the QCSE [see Fig. 1(c)] at which efficient generation of indirect excitons sets in. Using the same data as in Fig. 6(a) we plot the PL intensity and energy in Figs. 6(b) and 6(c), respectively, for both increasing $V_G$ (red trace) and decreasing $V_G$ (black trace). Accordingly, as displayed in Figs. 6(b) and 6(c), a relatively high intensity and energy of IX is recorded from the center of
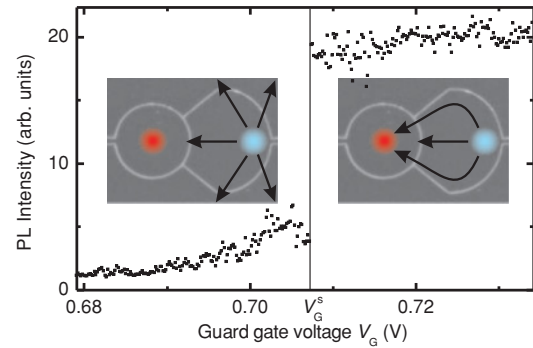


FIG. 7. (Color online) PL intensity at energy 1.40 eV ($\lambda =$ 886.0 nm) as a function of the guard gate voltage. The guard gate voltage is changed in increments of $\Delta V_G = 40$ $\mu$V between each data point. The laser power of 20 $\mu$W is focused on the slide gate and $V_S = 0.575$ V and $V_T = 0.35$ V. The two insets show the IX flow in the potential landscape after and before the switching.

the trap at voltages $V_G \gg V_S, V_T$ where efficient confinement of IX is realized. However, once $V_G$ is decreased below a threshold $V_G^s$ we observe an abrupt decrease of both the IX energy and intensity in the trap reflecting a sudden loss of IX in the trap. Utilizing spatially resolved PL microscopy as in Fig. 2, we verify that this loss occurs whenever the confinement of IX on the slide is lost with decreasing $V_G$. We note that no such switching behavior is observed when $V_G$ is increased from a value below $V_G^s$. At $V_G > V_G^s$ and sufficiently high generation rate on the slide, a large flow of IX from the slide to the trap causes a strong population of the trap, as reflected by a blueshift and a high PL intensity from IX, as illustrated in the inset on the right-hand side of Fig. 7. At threshold $V_G^s$ confinement of IX on the slide is lost such that the flow of IX from the slide to the trap is suddenly reduced, resulting in a downward jump in the PL intensity and blueshift, as illustrated in Fig. 6 and on the left-hand side in Fig. 7. By reversing the direction of the $V_G$ sweep, the missing excitonic confinement on the slide prevents a strong buildup of IX population in the trap, as shown in the red trace in Figs. 6(b) and 6(c) for $V_G > V_G^s$.

In the left part of Fig. 6 we also observe a regime of decreasing $V_G$ with $V_T < V_G < V_S$ in which the population in the trap builds up again before vanishing once $V_G < V_T$. This behavior is nonhysteretic and indicates that IX generated on the slide and transferred under the guard gate are partly collected in the trap whenever $V_G$ approaches $V_T$. This implies that IX from under the guard gate become sufficiently long lived and mobile to reach the fringe fields of the trap ($V_G < V_{kink}$). This happens as the QCSE redshifts the PL under the guard gate as seen in the intensity and energy trace in the left part of Figs. 6(b) and 6(c). With further decreasing $V_G$ the corresponding excitonic potential drops below the one of the trap and thus the trap gets depleted of IX.

The switching instability at $V_G^s$ is further illustrated in Fig. 7, where the PL intensity at an emission energy of 1.40 eV ($\lambda \equiv 886$ nm) is plotted with stepwise reducing of $V_G$ in increments of $\Delta V_G = 40$ $\mu$V. A single step in $V_G$ reduces the PL intensity at the trap center by about a factor of three as excitons are transferred to the region under the guard gate instead of the trap (see insets in
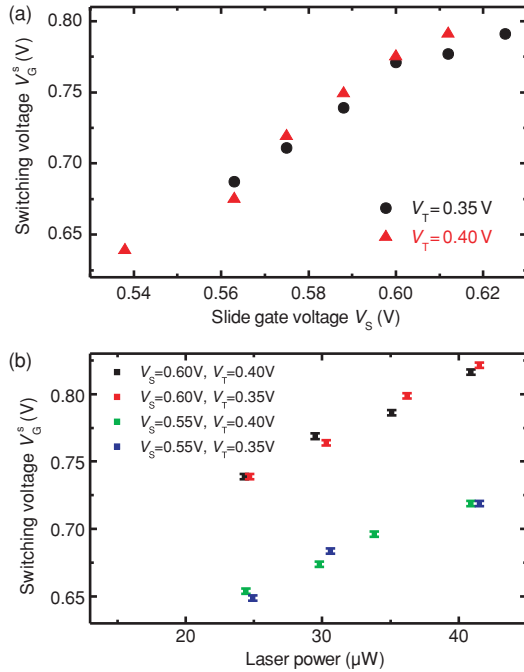
FIG. 8. (Color online) (a) Dependence of the switching voltage $V_G^s$ on the slide gate voltage $V_S$ and (b) the incident laser power for slide gate voltages of $V_S = 0.55$ V and $V_S = 0.6$ V. Variation of $V_T$ from 0.35 V to 0.4 V shows no significant influence in (a) and (b).

Fig. 7). Similar gate-controlled excitonic switching behavior and flux control has been reported previously[38–40] and refereed to as an "exciton optoelectronic transistor," an example of an "excitonic integrated circuit" where the exciton flow is controlled by a gate between "source" and "drain." In our device the flow of IX from source (slide) to drain (trap) is controlled by the bias $V_G$ of the guard gate as illustrated in Fig. 7.

Figure 8 summarizes the dependence of the switching voltage $V_G^s$ on the bias of the slide gate $V_S$ and the laser power incident onto the spot of electron-hole pair generation on the slide for two values of $V_T$. Figure 8(a) displays $V_G^s$ versus $V_S$ at an incident laser power of 20 $\mu$W and shows that $V_G^s$ increases nearly linearly with $V_S$ until it saturates close to the flat band voltage $V_{FB}$. No significant dependence on $V_T$ is seen. The population switching is only observed at slide gate voltages $V_S$ with 0.53 V $\lesssim V_S \lesssim$ 0.63 V, i.e., in the regime around the voltage kink in the QCSE [see Fig. 1(c)] at which a strong increase of the exciton population occurs under the slide gate. In contrast the population switching appears only above $V_G^s \gtrsim$ 0.64 V, i.e., in the voltage regime where no strong IX population occurs under the guard gate. Increasing the incident laser power [Fig. 8(b)], one finds a nearly linear increase of the switching voltage $V_G^s$ with its value depending on $V_S$ but not on $V_T$. Such a linear increase can be interpreted as reflecting a linear increase in IX density and a corresponding blueshift of the IX energy. Accordingly, the switching voltage $V_G^s$ is shifted upward.

In the above discussion we have omitted the potential effect of the geometric opening of about 100 nm between the gates needed for isolation. There, the Fermi level pinning of a

free GaAs surface at midenergy gap introduces an additional excitonic barrier, preventing somewhat the immediate flow of excitons between gates biased at the same voltage. We expect some minor effect of this opening on the switching behavior but have omitted it from the above discussion as it is rather difficult to quantify. The abruptness of the switching might be enhanced by effects of illumination reaching the opening. Additionally we cannot exclude some influence of "free" electrons confined under the guard gate for $V_G > V_{kink}$ on the switching behavior.

## VI. TUNING THE EXCITON DENSITY IN THE TRAP

We now explore the tunability of the exciton density in the trap with illumination intensity while operating at fixed gate voltage settings of $V_T = 0.38$ V, $V_S = 0.43$ V, and $V_G = 0.8$ V, close to where the optimum filling of the trap can be achieved. We vary the incident laser power focused on the slide as in Fig. 2(b) quasistatically by tuning the power transmitted into the microscope with an acousto-optical modulator. It thus is possible to change the excitation power by three orders of magnitude. The corresponding change in PL energy and intensity of the IX as collected from the trap center is displayed in Fig. 9(a). The PL energy initially rises steeply with increasing laser power and then approaches a saturation value. The PL intensity integrated over the IX line shape behaves distinctly differently as it starts with a slow rise and then, at an incident power of and above ~5 $\mu$W, rises linearly with laser power. This difference in behavior becomes amplified as we plot in Fig. 9(b) the PL intensity versus the PL blueshift employing the same data as in Fig. 9(a), both on a linear scale [black left-hand side of Fig. 9(b)] and on a logarithmic scale [red right-hand side of Fig. 9(b)]. We assume the blueshift of the PL energy to be proportional to the density of IX as in Eq. (1) to obtain the density values given at the top of Fig. 9(b). This linear relation is likely to underestimate the total IX density by about $2 \times 10^{10}$ $\frac{1}{cm^2}$ as discussed in Sec. II. This, however, cannot explain the strong nonlinear relation between PL intensity and PL blueshift seen in Fig. 9(b). The logarithmically plotted intensity suggests an exponential rise of the PL intensity with density, at least at low excitation powers. A possible explanation could be the action of the random disorder potential, which tends to spatially separate electron and hole wave function in the CDQW plane and thus suppresses luminescence at low densities. Possibly at these higher densities collective behavior, such as the screening of a random potential in a trap and exciton-exciton interaction, starts to be of some importance. In particular, the exciton binding energy is expected to decrease at high exciton densities because of screening and scattering in an exciton gas. This can increase the exciton radius and also weaken the exciton oscillator strength. This may contribute to the behavior of PL intensity at high pumping intensities (Fig. 9). In Fig. 9(a), the PL energy depends sublinearly on laser power, whereas the PL intensity is close to a linear function, except at small powers. Assuming that the PL energy reflects the IX density, then, one concludes that the IX density in a trap tends to become saturated at high laser powers (or correspondingly high IX densities).
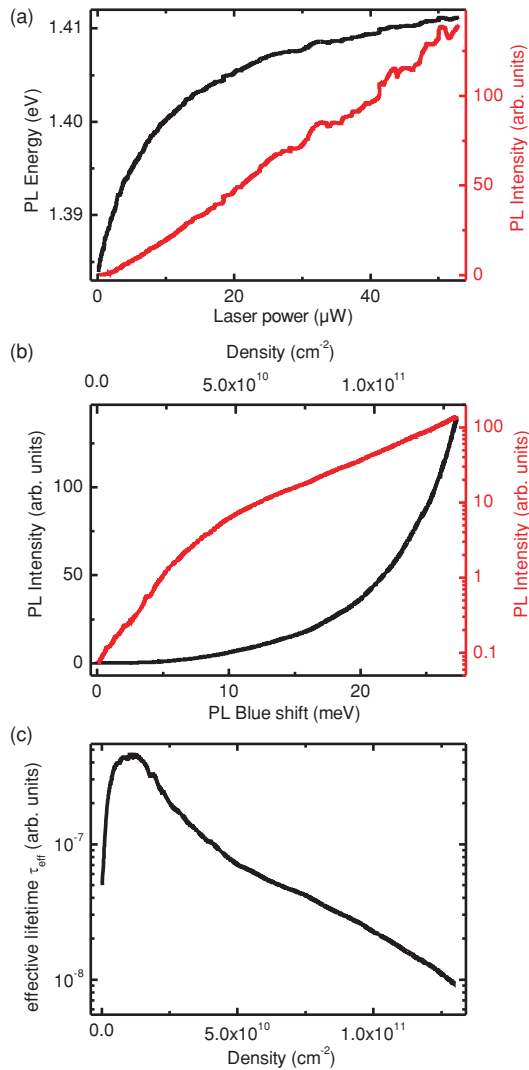
FIG. 9. (Color online) The indirect exciton density in the trap is changed by laser power. In (a) are plotted the PL energy and blueshift (black, left-hand axis) and the intensity (red, right-hand axis) of the trapped excitons as a function of the laser power on the slide gate. The same data are shown in (b) with the PL intensity plotted as a function of the PL blueshift. The linearly scaled PL intensity is shown in black and refers to the scale on the left-hand side and the logarithmically scaled PL intensity in red refers to the scale on the right-hand side. In (c) is plotted the effective exciton lifetime extracted from the data shown in (a) and (b) as a function of the exciton density.

The observations in Figs. 9(a) and 9(b) can also be interpreted in terms of an effective exciton lifetime. Assuming a simple rate equation for the total exciton population $N$ in a trap, $dN/dt = P - N/\tau_{\mathrm{eff}} = 0$, we obtain $\tau_{\mathrm{eff}} = N/P$, where $P$ is the rate of exciton feeding of the trap. Then, we assume that all excitons radiate and therefore $I_{\mathrm{PL}} \sim P$, where $I_{\mathrm{PL}}$ is the PL intensity. In a simplified approach, $N$ is proportional to the energy blueshift ($\Delta E$). In the next step, this naive model gives us $\tau_{\mathrm{eff}} = N/P \sim \Delta E/I_{\mathrm{PL}}$. Since $I_{\mathrm{PL}}$ grows nearly linearly with laser power and hence faster than the PL energy shift $\Delta E$ [Fig. 9(a)], the ratio $\Delta E/I_{\mathrm{PL}}$ and hence $\tau_{\mathrm{eff}}$ decreases with increasing laser power and equivalently

increasing $N$. Such behavior is reflected in Fig. 9(c) at not too low exciton densities in the trap where $\tau_{\mathrm{eff}}$ versus the exciton density is plotted using the same data as in Figs. 9(a) and 9(b). This observations can be explained as follows: With increasing exciton density the exciton energy is blueshifted ($\Delta E$) because of the screening of the externally applied electric field. The consequence is a strongly increasing overlap of the tails of the electron and hole wave functions forming the IX (at nearly constant dipole moment), thus resulting in a shorter lifetime. In simulations of the electron and hole wave function we can verify this behavior. Additionally, in experiments lifetimes vary between nanoseconds[30] for DX (maximum overlap of the wave functions) and up to microseconds[31] for IX. The lifetime decrease obtained in Fig. 9(c) at lowest densities $\leqslant 2 \times 10^{10} \frac{1}{\mathrm{cm}^2}$ is likely to be an artifact, reflecting that $N \sim \Delta E$ is no longer valid as discussed above. An additional influence might result from the random disorder potential expected to have a larger amplitude in InGaAs alloy than in pure GaAs.

Finally we want to point out that the tunability of the IX density of up to $1.3 \times 10^{11} \frac{1}{\mathrm{cm}^2}$ covers the regime of interest where the interexciton distance is still somewhat larger than the excitonic Bohr radius. In this regime, the thermal wavelength of excitons can be expected to become comparable to their distance at temperatures of order 1 K and below. This motivates us strongly to carry out future experiments to lower temperatures.

## VII. CONCLUSION

In our present studies we have realized a trapping scheme for spatially indirect excitons in coupled quantum wells that is well suitable for the exploration of excitonic many-body and condensation phenomena. We generate spatially indirect excitons in the focal spot of a relatively low power laser and we use spatial control of the quantum confined Stark effect via suitable patterned and biased gates to transfer IX from the focal spot on the slide gate to an electrostatically tunable trap. The trap provides an attractive excitonic potential but prevents the accumulation of net charges. Using a guard gate surrounding both trap and slide allows us to control the effective excitonic trap depth and to realize efficient transfer of mobile IX from the illumination spot to the trap with well controllable excess energy. As the transfer time of IX to the trap of order 1 ns is significantly larger than the excitonic relaxation time via acoustic phonons we can expect the excitons in the trap to be in thermal equilibrium with the lattice. The achieved tunability of the IX density in the trap covers the regime in which we expect quasibosonic interaction of indirect excitons. Additional cooling of the experiment by about 1 order of magnitude in temperature, which now is within experimental reach, is likely to transform the indirect excitonic ensemble into a condensate. Nevertheless, an additional challenge remains in identifying suitable techniques such as spatial narrowing of the light emission,[41,42] spectral narrowing of the emission, interference phenomena,[5] superfluidity,[8,43] and vertices[42,44] to detect the transition to a BEC-like condensate.

[1] L. V. Keldysh and A. N. Kozlov, Sov. Phys. JETP **27**, 521 (1968) [Zh. Eksp. Teor. Fiz. **54**, 978 (1968)].

[2] S. Yang, A. T. Hammack, M. M. Fogler, L. V. Butov, and A. C. Gossard, Phys. Rev. Lett. **97**, 187402 (2006).

[3] A. V. Gorbunov and V. B. Timofeev, JETP Lett. **83**, 146 (2006).

[4] S. O. Demokritov, V. E. Demidov, O. Dzyapko, G. A. Melkov, A. A. Serga, B. Hillebrands, and A. N. Slavin, Nature (London) **443**, 430 (2006).

[5] J. Kasprzak, M. Richard, S. Kundermann, A. Baas, P. Jeambrun, J. M. J. Keeling, F. M. Marchetti, M. H. Szymańska, R. André, J. L. Staehli, *et al.*, Nature (London) **443**, 409 (2006).

[6] H. Deng, H. Haug, and Y. Yamamoto, Rev. Mod. Phys. **82**, 1489 (2010).

[7] W. Ketterle and N. J. van Druten, Phys. Rev. A **54**, 656 (1996).

[8] D. S. Petrov, M. Holzmann, and G. V. Shlyapnikov, Phys. Rev. Lett. **84**, 2551 (2000).

[9] D. P. Trauernicht, A. Mysyrowicz, and J. P. Wolfe, Phys. Rev. B **28**, 3590 (1983).

[10] K. Kash, J. M. Worlock, M. D. Sturge, P. Grabbe, J. P. Harbison, A. Scherer, and P. S. D. Lin, Appl. Phys. Lett. **53**, 782 (1988).

[11] V. Negoita, D. W. Snoke, and K. Eberl, Appl. Phys. Lett. **75**, 2059 (1999).

[12] L. V. Butov, C. W. Lai, A. L. Ivanov, A. C. Gossard, and D. S. Chemla, Nature (London) **417**, 47 (2002).

[13] P. C. M. Christianen, F. Piazza, J. G. S. Lok, J. C. Maan, and W. van der Vleuten, Physica B **249-251**, 624 (1998).

[14] J. A. H. Stotz, R. Hey, P. V. Santos, and K. H. Ploog, Nature Mater. **4**, 585 (2005).

[15] A. T. Hammack, M. Griswold, L. V. Butov, L. E. Smallwood, A. L. Ivanov, and A. C. Gossard, Phys. Rev. Lett. **96**, 227402 (2006).

[16] S. Zimmermann, A. O. Govorov, W. Hansen, J. P. Kotthaus, M. Bichler, and W. Wegscheider, Phys. Rev. B **56**, 13414 (1997).

[17] S. Zimmermann, G. Schedelbeck, A. O. Govorov, A. Wixforth, J. P. Kotthaus, M. Bichler, W. Wegscheider, and G. Abstreiter, Appl. Phys. Lett. **73**, 154 (1998).

[18] T. Huber, A. Zrenner, W. Wegscheider, and M. Bichler, Phys. Status Solidi A **166**, 5 (1998).

[19] R. Rapaport, G. Chen, S. Simon, O. Mitrofanov, L. Pfeiffer, and P. M. Platzman, Phys. Rev. B **72**, 075428 (2005).

[20] V. B. Timofeev and A. V. Gorbunov, J. Appl. Phys. **101**, 081708 (2007).

[21] A. T. Hammack, N. A. Gippius, S. Yang, G. O. Andreev, L. V. Butov, M. Hanson, and A. C. Gossard, J. Appl. Phys. **99**, 066104 (2006).

[22] G. Chen, R. Rapaport, L. N. Pffeifer, K. West, P. M. Platzman, S. Simon, Z. Vörös, and D. Snoke, Phys. Rev. B **74**, 045309 (2006).

[23] A. A. High, A. T. Hammack, L. V. Butov, L. Mouchliadis, A. L. Ivanov, M. Hanson, and A. C. Gossard, Nano Lett. **9**, 2094 (2009).

[24] A. A. High, A. K. Thomas, G. Grosso, M. Remeika, A. T. Hammack, A. D. Meyertholen, M. M. Fogler, L. V. Butov, M. Hanson, and A. C. Gossard, Phys. Rev. Lett. **103**, 087403 (2009).

[25] A. Gärtner, L. Prechtel, D. Schuh, A. W. Holleitner, and J. P. Kotthaus, Phys. Rev. B **76**, 085304 (2007).

[26] X. P. Vögele, D. Schuh, W. Wegscheider, J. P. Kotthaus, and A. W. Holleitner, Phys. Rev. Lett. **103**, 126402 (2009).

[27] T. C. Damen, J. Shah, D. Y. Oberli, D. S. Chemla, J. E. Cunningham, and J. M. Kuo, Phys. Rev. B **42**, 7434 (1990).

[28] M. Gulia, F. Rossi, E. Molinari, P. E. Selbmann, and P. Lugli, Phys. Rev. B **55**, R16049 (1997).

[29] A. T. Hammack, L. V. Butov, J. Wilkes, L. Mouchliadis, E. A. Muljarov, A. L. Ivanov, and A. C. Gossard, Phys. Rev. B **80**, 155331 (2009).

[30] J. Feldmann, G. Peter, E. O. Göbel, P. Dawson, K. Moore, C. Foxon, and R. J. Elliot, Phys. Rev. Lett. **59**, 2337 (1987).

[31] Z. Vörös, D. W. Snoke, L. Pfeiffer, and K. West, Phys. Rev. Lett. **103**, 016403 (2009).

[32] M. H. Szymanska and P. B. Littlewood, Phys. Rev. B **67**, 193305 (2003).

[33] M. Stern, V. Garmider, V. Umansky, and I. Bar-Joseph, Phys. Rev. Lett. **100**, 256402 (2008).

[34] C. Schindler and R. Zimmermann, Phys. Rev. B **78**, 045313 (2008).

[35] A. L. Ivanov, E. A. Muljarov, L. Mouchliadis, and R. Zimmermann, Phys. Rev. Lett. **104**, 179701 (2010).

[36] A. Högele, S. Seidl, M. Kroner, K. Karrai, C. Schulhauser, O. Sqalli, J. Scrimgeour, and R. J. Warburton, Rev. Sci. Instrum. **79**, 023709 (2008).

[37] M. Stern, V. Garmider, E. Segre, M. Rappaport, V. Umansky, Y. Levinson, and I. Bar-Joseph, Phys. Rev. Lett. **101**, 257402 (2008).

[38] A. A. High, A. T. Hammack, L. V. Butov, M. Hanson, and A. C. Gossard, Opt. Lett. **32**, 2466 (2007).

[39] A. A. High, E. E. Novitskaya, L. V. Butov, M. Hanson, and A. C. Gossard, Science **321**, 229 (2008).

[40] Y. Y. Kuznetsova, M. Remeika, A. A. High, A. T. Hammack, L. V. Butov, M. Hanson, and A. C. Gossard, Opt. Lett. **35**, 1587 (2010).

[41] R. Balili, V. Hartwell, D. Snoke, L. Pfeiffer, and K. West, Science **316**, 1007 (2007).

[42] J. Keeling, L. S. Levitov, and P. B. Littlewood, Phys. Rev. Lett. **92**, 176402 (2004).

[43] A. V. Balatsky, Y. N. Joglekar, and P. B. Littlewood, Phys. Rev. Lett. **93**, 266801 (2004).

[44] K. G. Lagoudakis, M. Wouters, M. Richard, A. Baas, I. Carusotto, R. André, L. S. Dang, and B. Deveaud-Plédran, Nature Phys. **4**, 706 (2008).